Research Square

Preprints are preliminary reports that have not undergone peer review.
They should not be considered conclusive, used to inform clinical practice,
or referenced by the media as validated information.

Ultrasound drives chemical systems out of equilibrium

Andreas Herrmann

herrmann@dwi.rwth-aachen.de

DWI – Leibniz Institute for Interactive Materials https://orcid.org/0000-0002-8886-0894

Marcus Lantzius-Beninga

Institute of Technical and Macromolecular Chemistry, RWTH Aachen University & DWI - Leibniz Institute for Interactive Materials https://orcid.org/0000-0003-1843-730X

Gurudas Chakraborty

DWI – Leibniz Institute for Interactive Materials

Chen Li

DWI – Leibniz Institute for Interactive Materials

Jens Köhler

DWI https://orcid.org/0000-0002-7881-1490

Article

Keywords:

Posted Date: December 26th, 2025

DOI: https://doi.org/10.21203/rs.3.rs-7856967/v1

License: This work is licensed under a Creative Commons Attribution 4.0 International License.
Read Full License

Additional Declarations: There is **NO** Competing Interest.

Abstract

Unlike most synthetic counterparts, living systems autonomously reorganize through continuous energy input and dissipation. Inspired by this principle, synthetic out-of-equilibrium reaction networks offer promising routes to self-regulating and reconfigurable systems. While chemical, light, and electrical inputs have been widely exploited, the use of mechanical energy to fuel dissipative chemistry remains unaddressed. Here, we harness ultrasound-generated mechanical energy, leveraging polymer mechanochemistry to drive dissipative reaction networks that regulate chemical functionalities. This strategy enables transient fluorophore activation, tunable near-infrared (NIR) emission, and catalysis directed by the spatial positioning of a macrocyclic rotaxane. Through in-situ fuel generation, we achieve time-programmed and dose-dependent propagation of reactions and activation of functions, establishing a mechanochemically governed, feed-forward pathway operating out of equilibrium. By coupling shear flow-induced mechanophore activation with systems chemistry, this work creates a unique framework for achieving remotely controlled, on-demand functionalities, and lays the foundation for a new paradigm, 'mechanodissipative chemistry'.

Main

Living systems operate far from thermodynamic equilibrium at the molecular scale, where energy-driven chemical fluxes violate the detailed balance characteristic of equilibrium states.[1] This continuous energy consumption enables them to build, remodel, and disassemble complex molecular architectures – such as microtubules assembled from tubulin,[2,3] crosslinked networks of actin filaments,[4,5] and the dynamic mitotic spindle[6] – that underpin essential biological functions. These energy-driven processes have inspired chemists to design artificial systems that likewise function out of equilibrium.[7–10] Such dissipative systems have been constructed from synthetic organic molecules,[11–14] from programmable biomacromolecular building blocks such as polynucleotides[15–17] and peptides[18,19], and from minimal building blocks[20,21], enabling the tailoring of structures and functions with molecular precision. This field of dissipative systems chemistry has been seminally advanced by establishing selection mechanisms for energy-dissipating out-of-equilibrium assemblies,[22] achieving molecular complexification of self-replicators,[23] and realizing controllable sustained oscillations in supramolecular compartments through the interplay of molecular and mesoscale processes.[24] Moreover, chemical reaction cycles[13] and enzymatic reaction networks[25–29] have been developed to drive and regulate out-of-equilibrium processes.

Building on molecular-level advances, dissipative chemistry has been seamlessly extended to the material scale – for example, Otto and co-workers coupled dissipative self-assembly with macroscopic fluid flows.[30] Likewise, Willner and co-workers achieved control over gels with dissipative, transient stiffness by switching transition metal oxidation states, further demonstrating how molecular events can translate into dynamic material properties.[31] Further research in this domain has demonstrated the fabrication of synthetic dissipative living materials[32] and the dissipative organization of

biomacromolecules within living cells[19], underscoring the potential to create systems with lifelike functionality[33] and to translate out-of-equilibrium control into the manipulation of cellular events.[34]

All the aforesaid dissipative systems fundamentally require chemical fuels to drive and sustain out-of-equilibrium states.[35] These fuels may be nature-inspired molecules such as ATP or GTP[36–38] or synthetic chemicals[11,12]. However, fuels are often externally added without precise control over the time and space dimensions of energy supply – unlike in living systems, where spatiotemporal regulation of energy input is a defining hallmark. Seminal studies by Prins and co-workers demonstrated the spatiotemporally controlled application of chemical fuel enabling dissipative assemblies for the development of synthetic active matter.[39,40] Both studies, however, relied on the local injection of molecules into a bulk hydrogel, a strategy that restricts adaptability to diverse environments due to possible damage of the gel and limited diffusion of the fuel within the network. In regard to external control, light[41–44], electricity[45–47], and combinations thereof[48] have been utilized, highlighting the importance of remotely addressable fuels for the precise manipulation of dissipative assemblies. Additionally, a dissipative system driven by two orthogonal stimuli of different natures – namely chemical and radiative – has been demonstrated, underscoring the potential for incorporating multi-stimuli-encoded temporal control into molecular-scale chemistry operating far from thermodynamic equilibrium.[49]

However, current external triggers suffer from various drawbacks. Light can degrade chemical compounds and interfere with optical functionalities and readouts[50,51], and its limited penetration depth poses a major challenge for applications in turbid media or larger reaction vessels[41,52]. Electricity-fueled dissipative systems, on the other hand, can suffer from electrode degradation[53] and require sophisticated experimental setups[47]. Moreover, electricity can directly interfere with redox-active compounds and catalytic transformations, as well as affect sensitive species such as fluorophores.[54]

Ultrasound, in contrast, provides a non-invasive, highly penetrative, and remotely addressable means to drive specific chemical transformations.[55–57] Owing to these features, solution-phase polymer mechanochemistry has rapidly advanced as a field focused on harnessing mechanical energy to drive productive and sustainable chemistry.[58–61] To exploit the mechanical force generated by cavitation bubble collapse, a wide variety of mechanochemically responsive motifs (mechanophores) have been developed[62] and incorporated into synthetic polymers to trigger distinct functions. These include catalysis[63–65], cross-linking[66,67], small molecule release[68–72], visual reporting of material damage[73,74], and drug as well as biomolecule (nucleic acids and proteins) activation.[75–79] Altogether, polymer mechanochemistry benefits from ultrasound as an efficient and precise external trigger that operates without interfering with small molecules of low contour length.[80,81] This selective sensing of force at the molecular level to control the release of desired molecules, and thereby their reactivity, offers an unprecedented opportunity. Thus, ultrasound was envisioned to enable the in-situ generation of chemical fuels for controlled manipulation of dissipative chemistry.

In this work, we couple mechanophore activation induced by elongational flow produced by inertial cavitation with the fundamental requirement of chemical fuels to drive and sustain out-of-equilibrium states in dissipative systems. In particular, we devised mechanochemically governed chemical reaction networks that convert mechanical energy into chemical energy via ultrasound-induced cleavage of disulfide mechanophores. The resulting thiols initiate a cascade encompassing proton release from a molecular switch (Fig. 1a) and, depending on the network design, trigger distinct latent functionalities, including transient fluorophore activation (Fig. 1b), tunable near-infrared (NIR) emission (Fig. 1c), or catalysis directed by the spatial positioning within a macrocyclic rotaxane (Fig. 1d). In regard to optical properties, we demonstrate dose-dependent, transient activation of a naphthalimide fluorophore. Site-specific protonation enables manipulation of donor-acceptor quenching, thereby activating fluorescence. The system reverts to its initial state due to the presence of 1,5,7-triazabicyclo[4.4.0]dec-5-ene (TBD), an organic base. This cycle can be re-initiated by further ultrasound exposure, enabling the chemistry to operate dynamically under out-of-equilibrium conditions both in solution (Fig. 2) and in turbid media (Supplementary Fig. 8). The latter finding uniquely highlights the outstanding feature of ultrasound as an energy source for driving dissipative chemical transformations across diverse environments. Beyond switching on fluorescence, the mechanochemically governed pathway also transiently manipulates the excitation characteristics and NIR emission (> 730 nm) of perylene-based fluorophores (Fig. 3). To demonstrate the generic employability of the mechanodissipative principle, we realize force-controlled motion at the molecular scale by transiently positioning a macrocycle on the [2]rotaxane handle (Fig. 4). This remotely controllable molecular motility is subsequently leveraged to dictate a biomimetic organocatalytic transformation (Fig. 5). Altogether, we establish a novel framework for achieving temporally-controlled, on-demand functionalities through ultrasound-driven dissipative networks, thereby laying the foundation for ‘mechanodissipative chemistry’.

Results and discussion

Modular design of mechanochemically controlled reaction networks for transient functional outcomes

To harness ultrasound-generated mechanical energy for driving dissipative reaction networks, we designed a modular mechanochemical pathway that enables the unidirectional flow of molecular signals regulating distinct chemical functionalities (Fig. 1). An established disulfide mechanophore[69,70,75,77,78] was incorporated at the center of an amphiphilic poly(oligo(ethylene glycol) acrylate) (POEGA) polymer, and ultrasound was applied to generate thiols in-situ, thereby converting mechanical into chemical energy. To complement the mechanoresponsive polymer, an acridinium perchlorate compound was employed as a molecular switch and proton reservoir.[82] Upon reversible Michael-type addition of the thiol to the acridinium, perchloric acid is released to fuel the dissipative activation of fluorescence (Fig. 2), modulation of the optical behavior of perylene-based NIR emitters (Fig. 3), and catalysis directed by spatial positioning within a macrocyclic rotaxane (Figs. 4 and 5). Owing to the reversibility of protonation, the systems can revert to their initial state either over time or through the addition of a base to trap the proton.

Mechanochemically-fueled dissipative activation of fluorescence

To demonstrate the captioned process, we selected a naphthalimide fluorophore for its well characterized fluorescence properties (Fig. 2a). The molecular switch and the naphthalimide fluorophore were synthesized by adapting literature procedures.[82,83] Experimental details can be found in the Supplementary Information (SI). We first confirmed the cascaded fluorophore activation by the linear propagation of molecular signals through spectroscopic investigations, using propane thiol as a model fuel (Supplementary Fig. 1a). Proton nuclear magnetic resonance (^{1}H NMR, Supplementary Fig. 1b) evidenced the Thiol-Michael addition to acridinium perchlorate, followed by proton transfer to the fluorophore's amine group, which was confirmed by fluorescence measurements showing activated fluorescence (Supplementary Fig. 2). Subsequently, we investigated ultrasound-triggered fuel generation from POEGA (M_n = 106 kg·mol^{-1}, $Đ$ = 1.1; Supplementary Fig. 44), which was synthesized via Cu-mediated controlled radical polymerization and contains a chain-centered disulfide mechanophore. We first verified mechanochemical disulfide bond scission using a thiol-selective probe (Supplementary Fig. 3). This was further confirmed by the appearance of a half-molecular weight peak in size-exclusion chromatography following sonication (Supplementary Fig. 45). Upon fueling the cascaded fluorophore activation, the increase in fluorescence intensity at 460 nm exhibited a linear correlation with ultrasound exposure time (R^2 > 0.98, Fig. 2b). This strong correlation indicates dose-dependent fueling induced by ultrasound and suggests that a rate-determining step follows the mechanochemical thiol generation, which typically obeys first-order kinetics. To exclude any unintended influence of ultrasound on the observed fluorophore activation, we introduced a pre-sonicated POEGA into the reaction mixture, which yielded a fluorescence response (Supplementary Fig. 4) consistent with that observed under in-situ sonication, thereby confirming the mechanistic pathway. In contrast, the addition of a non-sonicated polymer produced no fluorescence change (Supplementary Fig. 5), underscoring the essential role of ultrasound as the energy input driving the process.

In the next step, to demonstrate the dissipative nature of the system, we investigated fluorophore deactivation and refueling-induced reactivation. Over several days (> 4 days), a modest decrease in fluorescence intensity was observed, which could be restored by subsequent ultrasound exposure (Fig. 1c). Conversely, in the presence of TBD, the system deactivated more rapidly (within 30 minutes) and showed fluorescence recovery upon refueling (Fig. 1d). It is worth noting that the basicity of the employed base is critical for base-induced deactivation, as the weaker base triethylamine (NEt_3) exhibited markedly different behavior compared to TBD (Supplementary Fig. 7). Monitoring the reversion of the fluorophore to the deactivated state over time, or in the presence of sub-stoichiometric amounts of an organic base, and its subsequent resetting via refueling highlights the system's dissipative character. These results provide the first evidence for our envisaged mechanochemically governed pathway enabling transient functional outcomes. To underscore the advantage of ultrasound as an energy source for driving dissipative chemical processes across diverse environments, particularly under conditions where light cannot operate effectively, we further investigated and successfully realized the

dissipative activation of the naphthalimide fluorophore in a turbid, colored reaction mixture (Supplementary Fig. 8).

Mechanodissipative switching of optical behavior of perylene-based NIR emitters

Following the in-situ production of fuels using ultrasound-generated mechanical energy and the establishment of dissipative fluorescence activation, we extended the scope of our mechanochemically governed pathway to enable switchable optical behavior of NIR emitters. Given the high tunability of the optical properties of perylene-based dyes, along with their amenability to asymmetric functionalization and incorporation into nano- and mesoscopic materials, we next investigated the transient modulation of the optical properties of perylene monoimide (PMI) amines.[84] PMI amines with red-shifted emission extending into the NIR region (λ > 720 nm) were specifically chosen, given their high relevance as a class of fluorophores,[85] to demonstrate the applicability of our mechanodissipative operating principle. For this purpose, we synthesized a reported PMI bearing a primary amine, as well as a novel PMI incorporating a tertiary amine (SI).[86,87] Subjecting the devised mechanochemical reaction network (vide supra), containing the primary or tertiary amines, to ultrasound leads to protonation of the amines and distinct changes in the photophysical properties of the fluorophores (Fig. 3a).

For the PMI primary amine, we show transient switching of the excitation spectrum between higher and lower wavelengths. While the excitation intensity increases at 380 nm (Fig. 3b) and ~520 nm (Supplementary Fig. 9), it decreases correspondingly at 600 nm (Fig. 3c). In addition, the NIR emission intensity mirrors the behavior of the higher-wavelength excitation profile and is transiently modulated upon ultrasound application (Fig. 3d). The dissipative switching of optical properties is further demonstrated by monitoring the excitation (Fig. 3e) and fluorescence (Fig. 3f) spectra. In the initial state and after dissipation, the excitation spectrum exhibits a broad, structureless profile, as expected for a charge-transfer transition between the amine and imide motifs.[88] In contrast, after ultrasound-driven fueling of the system, a structured excitation profile with a blue-shifted maximum is observed, attributed to the absence of the amine nitrogen lone pair.[88] Correspondingly, the fluorescence spectra of the initial and dissipated states exhibit only a red-shifted maximum, whereas in the fueled state, an additional emission maximum appears at 550-600 nm. These observations are consistent with earlier studies on fluorescence changes upon thermal deprotection to release PMI primary amines.[88] Altogether, our results demonstrate the ultrasound-induced transient modulation of the optical properties of perylene fluorophores. To highlight the versatility of this approach, we further investigated the transient optical behavior of a novel PMI tertiary amine, a structural analogue of the naphthalimide fluorophore used above, but featuring red-shifted excitation and fluorescence spectra (λ_{ex} = 540 nm, λ_{em} = 730 nm). Here, we demonstrate NIR emission activation while the positions of the excitation and emission maxima remain unaffected (Fig. 3g). Thus, ultrasound enables transient activation of the emissive state of the perylene dye, paving the way for externally regulatable dissipative NIR emitters for imaging and sensing.

Mechanochemically governed pathway for controlling transient motion at the molecular scale

In an effort to further expand the applicability of our mechanodissipative chemistry principle, we sought to control molecular motion in response to ultrasound-generated mechanical energy. To this end, we focused on modulating the transient positioning of the macrocycle in a [2]rotaxane, a prototypical example of a simple molecular machine.[89] First, we synthesized a novel [2]rotaxane comprising an organocatalytically active thiourea motif, a secondary amine serving as a transient anchor for the macrocycle, and a latent fluorescent cap acting as a sensor for macrocycle positioning. Anthracene was chosen for the cap due to its well-established utility as a macrocycle positioning sensor.[90] The synthesis of the novel [2]rotaxane was accomplished in five steps starting from commercially available materials, with full experimental details provided in the SI. The positioning of the macrocycle can be controlled by tuning the interaction strength between the macrocycle and the anchoring motifs. In the neutral state, the thiourea-macrocycle interaction dominates over that of the amine, whereas upon protonation of the amine, the trend reverses.[91] To harness mechanical energy for controlling macrocycle positioning, we subjected the corresponding reaction network to ultrasound (Fig. 4a).

Macrocycle positioning on the rotaxane handle was monitored by recording fluorescence spectra. Upon ultrasound-induced fueling, we observed an increase in fluorescence corresponding to the characteristic anthracene signal (Fig. 4b), indicating relocation of the macrocycle from the thiourea motif to the protonated amine. Control experiments, in which the reaction mixture was sonicated without the polymer as a thiol source, showed no change in anthracene fluorescence, highlighting the non-destructive nature of ultrasound even for complex functional compounds with relatively high molecular weights (> 1 $kg \cdot mol^{-1}$) (Supplementary Fig. 10). Beyond activating the reaction network to control transient motion at the molecular scale, we investigated the dissipation and refueling of the activated state. Dissipation was observed in the presence of different bases, and the system could be reactivated by ultrasound-induced refueling (TBD, Fig. 4c; NEt_3, Supplementary Fig. 11). These results provide unprecedented evidence for the applicability of force-induced in-situ generation and cascaded propagation of molecular signals in enabling the out-of-equilibrium operation of a molecular machine.

Mechanodissipative catalysis

Subsequently, we leveraged the force-governed transient motion at the molecular scale, described above, to modulate chemical catalysis. By controlling the macrocycle positioning, the ultrasound-fueled dissipative reaction network transiently unmasks the thiourea motif, allowing it to function as an organocatalyst in the biomimetic hydrogenation of nitrostyrene using a Hantzsch ester as the hydrogen donor (Fig. 5a). Upon fueling the reaction network, the macrocycle relocated to the amine motif, as indicated by ^1H NMR spectroscopy (Fig. 5b).[91] Over time, it reverted to its initial position, thereby deactivating the catalytic function. NMR served as a complementary technique to fluorescence spectroscopy for monitoring dissipative macrocycle positioning. To confirm the catalytic activity of the unmasked thiourea, we followed the hydrogenation reaction and determined the corresponding reaction rate constant (Supplementary Table 1; Supplementary Figs. 14-15). As expected, a minor background reaction occurred in the absence of fueling due to the uncatalyzed reaction between the two substrates.

Upon ultrasound stimulation, the reaction rate constant increased significantly, confirming the uncaging of the thiourea and rendering it catalytically active (Fig. 5c). Importantly, the generated acid fuel does not affect this biomimetic hydrogenation, and the observed reaction rate constants are in good agreement with previously reported values for a similar catalyst under non-mechanochemically activated conditions.[91] Consistent with the NMR data on ring positioning, the catalytic activity gradually returned to its initial level over time (Fig. 5d). Upon refueling, the catalytic activity was restored. Altogether, we conclude that the investigated systems highlight the potential of mechano-regulated dissipative pathways to trigger catalysis on demand, without interfering with other chemical functions or complex molecules. These findings introduce 'mechanodissipative catalysis' as a novel and distinct paradigm in catalysis.

Conclusion

In conclusion, this work uniquely demonstrates that ultrasound can activate chemical fuels as effective energy source to drive molecular systems far from thermodynamic equilibrium. This energy-harnessing strategy relies on a mechanochemically governed, feed-forward pathway that operates in accordance with the first law of thermodynamics, transforming mechanical energy into chemical input to achieve desired functional outcomes through the controlled propagation of molecular signals. Such propagation initiates a cascade involving proton release from a molecular switch and, depending on the network design, triggers distinct latent functionalities, including fluorophore activation, optical switching of NIR emitters, spatial positioning of a macrocycle in a [2]rotaxane, and modulation of the catalytic activity of a rotaxane-based organocatalyst. This was achieved by coupling mechanochemical thiol generation under elongational flow with the requirement of chemical fuels to sustain the out-of-equilibrium states necessary to drive these processes dissipatively. Owing to the principles of solution-based polymer mechanochemistry, the functional molecules (naphthalimide, perylene monoimides, and [2]rotaxane) remain protected from the energy source, preventing interference with their functional outcomes. To highlight the advantage of ultrasound as an energy source for driving dissipative chemical transformations in diverse environments, particularly under conditions where light is ineffective, we demonstrated the transient activation of the naphthalimide fluorophore in a turbid, colored reaction mixture. In a nutshell, we introduce a novel integration of two research fields, namely polymer mechanochemistry and dissipative systems chemistry, to establish a new paradigm, 'mechanodissipative chemistry'. This approach enables the in-situ generation of remotely addressable fuels for controlled manipulation of dissipative chemical networks. The principles of 'mechanodissipative chemistry' will enhance system autonomy and advance paradigms in domino[92] or cascade[93] catalytic processes. Beyond these applications, we envision that this new field will further progress supramolecular systems chemistry[94], force-controlled directed molecular motions[95], blinking and switchable NIR emitters with high relevance for in-vivo imaging[96–99], and the incorporation of dissipative chemical networks into bulk materials for externally controllable, localized operations.

Methods

Materials

Unless otherwise stated, all chemical reagents used in this study were of synthesis grade or higher purity and were used without further purification. Acridine (96%, Sigma Aldrich), aminomethyl anthracene (95-98%, BLDpharm), bis(3,5-trifluoromethyl)phenyl thioisocyanate (>98.0%, TCI), bis(2-(2'-bromoisobutyryloxy) ethyl)disulfide (Sigma Aldrich), boc-2-(4-aminophenyl)ethanol (97%, BLDpharm), bromine (Sigma Aldrich), 4-bromo-1,8-naphthylic anhydride (95%, abcr), copper(II) bromide (Sigma Aldrich), dibenzo-24-crown-8 (98%, Sigma Aldrich), diethyl-1,4-dihydro-2,6-dimethyl-3,5-pyridinedicarboxylate (Hantzsch ester, BLDpharm), diisopropyl aniline (97%, Sigma Aldrich), hydroxybenzyl aldehyde (>98%, TCI), imidazole (>99%, Sigma Aldrich), 2-methoxy ethylamine (96%, Sigma Aldrich), methyl iodide (99%, Thermo Fisher Scientific), methyl piperazine (>98%, Thermo Fisher Scientific), β-nitrostyrene (Sigma Aldrich), perylenetetracarboxylic dianhydride (97%, Sigma Aldrich), propane thiol (Sigma Aldrich), sodium azide (Sigma Aldrich), sodium borohydride (98%, abcr), sodium perchlorate (Thermo Fisher Scientific), trifluoromethane sulfonic acid chloride (Sigma Aldrich), tris(2-(dimethylamino)ethyl)amine (Me6TREN, >98.0%, TCI), and zinc acetate dihydrate (>99.0%, Sigma Aldrich) were used as received. Oligo(ethylene glycol) methyl ether acrylate (OEGA, Sigma Aldrich, $M_n \approx 480$ g·mol^{-1}) was passed through a column of basic aluminum oxide before polymerization to remove the inhibitor. The copper wire (d = 3 cm) was activated prior to use by stirring it in hydrochloric acid for 15 min, followed by thorough rinsing with methanol and ultrapure water, and drying under high vacuum prior to use.

Characterization and equipment

NMR spectra (^{1}H and ^{13}C) were recorded on a Bruker Avance 300, a Bruker Avance 400, or a Bruker Avance 600 spectrometer with a frequency of 300 MHz (^{13}C: 75 MHz), 400 MHz (^{13}C: 101 MHz), or 600 MHz (^{13}C: 151 MHz), respectively. Chemical shifts are reported as δ (ppm) using the residual peak of protonated solvents (chloroform-d: 7.26 ppm (^{1}H) and 77.2 ppm (^{13}C); dimethyl sulfoxide-d_6: 2.50 ppm (^{1}H) and 39.5 ppm (^{13}C); and toluene-d_8: 7.00 ppm (^{1}H). These were all purchased from Sigma Aldrich).[100] The following abbreviations were used throughout: s = singlet; d = doublet; t = triplet; q = quartet; sept. = septet; dd = doublet of doublets, etc.; and m = multiplet. All NMR spectra were processed and analyzed using automated phase correction and third-order binomial baseline correction in the MestreNova x64 software (Mestrelab Research). Thin-layer chromatography was performed using Polygram Sil-UV$_{254}$ TLC plates (Machery-Nagel), which are coated with silica 60 and a fluorescence indicator. For silica gel chromatography, silica 60 (0.063-0.2 mm, Machery-Nagel) was used. The [2]rotaxane was purified on a Bio-Rad resin (200-400 mesh). Molecular weights (M_n and M_w) and molecular weight distributions (M_w/M_n) were determined by size-exclusion chromatography (SEC). SEC analyses were carried out using tetrahydrofuran (THF) (≥99.7%, unstabilized, HiPerSolv CHROMANORM® HPLC grade, VWR) as the eluent. The machine was equipped with an HPLC pump (1260 Infinity II, Agilent Technologies), a refractive index detector (RID, 1260 Infinity II, Agilent Technologies), a UV-detector (VWD, 1260 Infinity II, Agilent Technologies), and a multi-angle light

scattering detector (MALS, SLD 7100, Polymer Standards Service). The samples contained 0.250 mg·mL^{-1} 3,5-di-*tert*-4-butylhydroxytoluene (BHT, ≥99%, Fluka) as the internal standard. One pre-column (4.6 × 50 mm) and four SDplus gel columns (4.6 × 300 mm, MZ Analysentechnik) were used with a flow rate of 0.35 mL·min^{-1} at 40 °C. The diameter of the gel particles was 5 µm and the nominal pore widths were 50, 10^2, 10^3, and 10^4 Å. Calibration was performed using narrowly distributed poly(methyl methacrylate) standards (Agilent Technologies). The average molecular weights (M_n and M_w) and the molecular weight distribution ($Đ = M_w/M_n$) were calculated using the PSS WinGPC UniChrom software (version 8.3.2). Electrospray ionization mass spectrometry (ESI MS) was performed using a micrOTOF-Q II™ ESI-Qq-TOF mass spectrometer system (Bruker). Matrix-assisted laser desorption and ionization time-of-flight (MALDI-ToF) MS was conducted in linear or reflection mode on a Daltonics Ultraflex II MALDI-ToF mass spectrometer (Bruker), which was equipped with a nitrogen laser that delivered 2 ns laser pulses at 337 nm. Positive ion ToF detection was performed using an accelerating voltage of 25 kV. The matrix solution was prepared by dissolving *trans*-2-(3-(4-*tert*-butylphenyl)-2-methyl-2-propenylidene) malononitrile (DCTB) in THF (10 mg·mL^{-1} solution). Fluorescence spectroscopy was performed using a Fluoromax 4P spectrometer (Horiba) with the indicated excitation and emission wavelengths in a quartz glass fluorescence cuvette with a 10 × 10 mm optical path length. For the normalized spectra, [0,1]-normalization was applied unless otherwise stated. Any background fluorescence was subtracted from the depicted spectra. All reactions were carried out using standard Schlenk techniques under an inert argon atmosphere.

Sonication experiments

Ultrasound irradiation experiments were carried out using a VibraCell^{TM} VCX500 ultrasonic processor (Sonics & Materials) with a 13 mm solid full-wave probe in a Suslick vessel (Sonics & Materials), under an inert atmosphere and cooling via an ice bath. A frequency of 20 kHz and an amplitude of 30% of the maximum amplitude (125 µm) were used for all experiments, with pulsed sonication applied (2.0 s on, 1.0 s off). The solutions prepared for the respective experiments (3 mL in dimethyl sulfoxide) were diluted with 15 mL of THF to ensure that the probe was immersed in the solution during the sonication experiment ($c_{Polymer}$ ≈ 0.5 mg·mL^{-1}). The resulting solutions were then degassed under a nitrogen flow for 10 min. After the ultrasound exposure for the desired time (0-30 min), the THF was removed under reduced pressure. If any solid particles were present, the solutions were filtered before further use. To ensure reproducibility, all samples were equilibrated for 30 min after the sonication before characterization by fluorescence or NMR spectroscopy.

Catalytic activity tests

The catalytic activity of the [2]rotaxane thiourea motif was determined in the organocatalytic conversion of β-nitrostyrene (0.025 M, 1.0 eq.) and Hantzsch ester (0.0275 M, 1.1 eq.) in a mixture of toluene-d_8/DMSO-d_6 (10:1, v/v) mixture with a catalyst loading of 10 mol%. The catalyst was fully deprotonated by stirring it for 30 min with a basic Amberlite IRA067 (OH^- form) ion exchange resin in dichloromethane.

Acridinium perchlorate (0.0075 M, 30 mol%) and the disulfide polymer (0.025 M, 100 mol%) were added to all samples. To determine the reaction rate in the absence of an uncaged catalyst, one set of samples was subjected to the same reaction conditions without applying ultrasound (background reaction rate). Reaction progress was monitored by ^{1}H NMR using tetramethyl silane (TMS) as the internal standard (0.1% v/v). To activate the catalytic function, the samples were treated with ultrasound for 10 min. After observing catalyst deactivation in the sonicated samples by NMR, the samples were subjected to ultrasound (10 min) again. The reaction rate was determined using second order kinetics and the corresponding linearization (c^{-1}), based on literature reports.[91] The reaction rate constant was determined by calculating the slope of the resulting linearized plots (c^{-1} vs. t). A t-test in the Origin2024b software (Origin Labs) was used to determine the statistically significant difference in the reaction rates in the OFF and ON states. The background reaction was subtracted for the representation of c_t/c_0 values.

Declarations

Acknowledgements

This research was supported by the EU through an ERC Advanced Grant (SONOPHARMAGEN, No. 101142296, to A.H.). Moreover, this work was funded as part of the Leibniz ScienceCampus: ACTISONO, supported by the Leibniz Association (No. W89/2023, to A.H.). The authors would like to thank Dr. Michael Pohl and Rainer Haas for SEC measurements, Marion Connolly for MALDI-ToF MS, and Petra Esser for ESI MS measurements. M.L-B. gratefully acknowledges support from the German Scholarship Foundation for a PhD scholarship.

Author Information

Authors and Affiliations

Institute of Technical and Macromolecular Chemistry, RWTH Aachen University, Forckenbeckstr. 50, 52074 Aachen, Germany

Marcus Lantzius-Beninga and Andreas Herrmann

DWI – Leibniz-Institute for Interactive Materials, Forckenbeckstr. 50, 52074 Aachen, Germany

Marcus Lantzius-Beninga, Gurudas Chakraborty, Chen Li, Jens Köhler, and Andreas Herrmann

Contributions

Conceptualization, M.L.B., G.C., and A.H.; Methodology, M.L.B., G.C., J.K., and A.H.; Investigation, M.L.B.; Writing – Original Draft, M.L.B. and G.C.; Writing – Review and Editing, M.L.B., G.C., and A.H.; Funding Acquisition, A.H.; Resources, C.L and A.H.; Supervision, G.C. and A.H.

Corresponding authors

Correspondence to Gurudas Chakraborty chakraborty@dwi.rwth-aachen.de or Andreas Herrmann herrmann@dwi.rwth-aachen.de.

Ethics declarations

The authors declare no competing financial interests.

References

1. Battle, C. *et al.* Broken detailed balance at mesoscopic scales in active biological systems. *Science* **352,** 604–607; 10.1126/science.aac8167 (2016).
2. Nédélec, F. J., Surrey, T., Maggs, A. C. & Leibler, S. Self-organization of microtubules and motors. *Nature* **389,** 305–308; 10.1038/38532; (1997).
3. Desai, A. & Mitchison, T. J. Microtubule polymerization dynamics. *Annu. Rev. Cell Dev. Biol.* **13,** 83–117; 10.1146/annurev.cellbio.13.1.83 (1997).
4. Tseng, Y. *et al.* How actin crosslinking and bundling proteins cooperate to generate an enhanced cell mechanical response. *Biochem. Biophys. Res. Commun.* **334,** 183–192; 10.1016/j.bbrc.2005.05.205 (2005).
5. Köhler, S., Schaller, V. & Bausch, A. R. Structure formation in active networks. *Nat. Mater.* **10,** 462–468; 10.1038/nmat3009 (2011).
6. O'Connell, C. B. & Khodjakov, A. L. Cooperative mechanisms of mitotic spindle formation. *J. Cell Sci.* **120,** 1717–1722; 10.1242/jcs.03442 (2007).
7. Whitesides, G. M. & Grzybowski, B. Self-assembly at all scales. *Science* **295,** 2418–2421; 10.1126/science.1070821 (2002).
8. Boekhoven, J., Hendriksen, W. E., Koper, G. J. M., Eelkema, R. & van Esch, J. H. Transient assembly of active materials fueled by a chemical reaction. *Science* **349,** 1075–1079; 10.1126/science.aac6103 (2015).
9. van Rossum, S. A. P., Tena-Solsona, M., van Esch, J. H., Eelkema, R. & Boekhoven, J. Dissipative out-of-equilibrium assembly of man-made supramolecular materials. *Chem. Soc. Rev.* **46,** 5519–5535; 10.1039/C7CS00246G (2017).
10. De, S. & Klajn, R. Dissipative Self-Assembly Driven by the Consumption of Chemical Fuels. *Adv. Mater.* **30,** e1706750; 10.1002/adma.201706750 (2018).
11. Boekhoven, J. *et al.* Dissipative self-assembly of a molecular gelator by using a chemical fuel. *Angew. Chem. Int. Ed.* **49,** 4825–4828; 10.1002/anie.201001511 (2010).
12. Tena-Solsona, M. *et al.* Non-equilibrium dissipative supramolecular materials with a tunable lifetime. *Nat. Commun.* **8,** 15895; 10.1038/ncomms15895 (2017).

13. Rieß, B., Grötsch, R. K. & Boekhoven, J. The Design of Dissipative Molecular Assemblies Driven by Chemical Reaction Cycles. *Chem.* **6,** 552–578; 10.1016/j.chempr.2019.11.008 (2020).
14. Del Giudice, D. & Di Stefano, S. Dissipative Systems Driven by the Decarboxylation of Activated Carboxylic Acids. *Acc. Chem. Res.* **56,** 889–899; 10.1021/acs.accounts.3c00047 (2023).
15. Luo, M. *et al.* Four-Dimensional Deoxyribonucleic Acid-Gold Nanoparticle Assemblies. *Angew. Chem. Int. Ed.* **59,** 17250–17255; 10.1002/anie.202007616 (2020).
16. Liu, Q. *et al.* DNA-Based Dissipative Assembly toward Nanoarchitectonics. *Adv. Funct. Mater.* **32,** 2201196; 10.1002/adfm.202201196 (2022).
17. Del Grosso, E., Franco, E., Prins, L. J. & Ricci, F. Dissipative DNA nanotechnology. *Nat. Chem.* **14,** 600–613; 10.1038/s41557-022-00957-6 (2022).
18. Debnath, S., Roy, S. & Ulijn, R. V. Peptide nanofibers with dynamic instability through nonequilibrium biocatalytic assembly. *J. Am. Chem. Soc.* **135,** 16789–16792; 10.1021/ja4086353 (2013).
19. Wang, H. *et al.* Organelle-Mediated Dissipative Self-Assembly of Peptides in Living Cells. *J. Am. Chem. Soc.* **146,** 330–341; 10.1021/jacs.3c09202 (2024).
20. Reja, A. *et al.* Feedback driven autonomous cycles of assembly and disassembly from minimal building blocks. *Nat. Commun.* **15,** 9980; 10.1038/s41467-024-54197-y (2024).
21. Afrose, S. P. *et al.* Minimal catalytic dissipative assemblies via cooperation of an amino acid, a nucleobase precursor and a cofactor. *Chem. Sci.* **16,** 7838–7846; 10.1039/D5SC00827A (2025).
22. Tena-Solsona, M., Wanzke, C., Riess, B., Bausch, A. R. & Boekhoven, J. Self-selection of dissipative assemblies driven by primitive chemical reaction networks. *Nat. Commun.* **9,** 2044; 10.1038/s41467-018-04488-y (2018).
23. Yang, S. *et al.* Chemical Fueling Enables Molecular Complexification of Self-Replicators. *Angew. Chem. Int. Ed.* **60,** 11344–11349; 10.1002/anie.202016196 (2021).
24. Howlett, M. G., Engwerda, A. H. J., Scanes, R. J. H. & Fletcher, S. P. An autonomously oscillating supramolecular self-replicator. *Nat. Chem.* **14,** 805–810; 10.1038/s41557-022-00949-6 (2022).
25. Sarkar, A., Dúzs, B. & Walther, A. Fuel-Driven Enzymatic Reaction Networks to Program Autonomous Thiol/Disulfide Redox Systems. *J. Am. Chem. Soc.* **146,** 10281–10285; 10.1021/jacs.4c02680 (2024).
26. Seo, H. & Lee, H. Programmable Enzymatic Reaction Network in Artificial Cell-Like Polymersomes. *Adv. Sci.* **11,** e2305760; 10.1002/advs.202305760 (2024).
27. Sharma, S., Belluati, A., Kumar, M. & Dhiman, S. Enzymatic Reaction Network-Driven Polymerization-Induced Transient Coacervation. *Angew. Chem. Int. Ed.* **64,** e202421620; 10.1002/anie.202421620 (2024).
28. Itatani, M. *et al.* Temporal pH waveforms generated in an enzymatic reaction network in batch and cell-sized microcompartments. *Cell Rep. Phys. Sci.* **6,** 102367; 10.1016/j.xcrp.2024.102367 (2025).
29. Deng, J. & Walther, A. Autonomous DNA nanostructures instructed by hierarchically concatenated chemical reaction networks. *Nat. Commun.* **12,** 5132; 10.1038/s41467-021-25450-5 (2021).

30. Liu, K. *et al.* Molecular-scale dissipative chemistry drives the formation of nanoscale assemblies and their macroscale transport. *Nat. Chem.* **17,** 124–131; 10.1038/s41557-024-01665-z (2025).
31. Baretta, R., Davidson-Rozenfeld, G., Gutkin, V., Frasconi, M. & Willner, I. Chemical and Photochemical-Driven Dissipative Fe3+/Fe2+-Ion Cross-Linked Carboxymethyl Cellulose Gels Operating Under Aerobic Conditions: Applications for Transient Controlled Release and Mechanical Actuation. *J. Am. Chem. Soc.* **146,** 9957–9966; 10.1021/jacs.4c00625 (2024).
32. Jo, H., Selmani, S., Guan, Z. & Sim, S. Sugar-Fueled Dissipative Living Materials. *J. Am. Chem. Soc.* **145,** 1811–1817; 10.1021/jacs.2c11122 (2023).
33. Shklyaev, O. E. & Balazs, A. C. Interlinking spatial dimensions and kinetic processes in dissipative materials to create synthetic systems with lifelike functionality. *Nat. Nanotechnol.* **19,** 146–159; 10.1038/s41565-023-01530-z (2024).
34. Xu, Y. *et al.* Dynamic Modulation of Multicellular Interactions via ATP-Dissipative DNA Assembly. *J. Am. Chem. Soc.* **147,** 28277–28288; 10.1021/jacs.5c08925 (2025).
35. Das, K., Gabrielli, L. & Prins, L. J. Chemically Fueled Self-Assembly in Biology and Chemistry. *Angew. Chem. Int. Ed.* **60,** 20120–20143; 10.1002/anie.202100274 (2021).
36. Maiti, S., Fortunati, I., Ferrante, C., Scrimin, P. & Prins, L. J. Dissipative self-assembly of vesicular nanoreactors. *Nat. Chem.* **8,** 725–731; 10.1038/nchem.2511 (2016).
37. Deng, J. & Walther, A. ATP-Responsive and ATP-Fueled Self-Assembling Systems and Materials. *Adv. Mater.* **32,** e2002629; 10.1002/adma.202002629 (2020).
38. Te Brinke, E. *et al.* Dissipative adaptation in driven self-assembly leading to self-dividing fibrils. *Nat. Nanotechnol.* **13,** 849–855; 10.1038/s41565-018-0192-1 (2018).
39. Kar, H., Goldin, L., Frezzato, D. & Prins, L. J. Local Self-Assembly of Dissipative Structures Sustained by Substrate Diffusion. *Angew. Chem. Int. Ed.* **63,** e202404583; 10.1002/anie.202404583 (2024).
40. Kar, H., Chen, R., Das, K. & Prins, L. J. Transient transition from Stable to Dissipative Assemblies in Response to the Spatiotemporal Availability of a Chemical Fuel. *Angew. Chem. Int. Ed.* **64,** e202414495; 10.1002/anie.202414495 (2025).
41. Weißenfels, M., Gemen, J. & Klajn, R. Dissipative Self-Assembly: Fueling with Chemicals versus Light. *Chem.* **7,** 23–37; 10.1016/j.chempr.2020.11.025 (2021).
42. Rizzuto, F. J. *et al.* A dissipative pathway for the structural evolution of DNA fibres. *Nat. Chem.* **13,** 843–849; 10.1038/s41557-021-00751-w (2021).
43. Wimberger, L., Rizzuto, F. J. & Beves, J. E. Modulating the Lifetime of DNA Motifs Using Visible Light and Small Molecules. *J. Am. Chem. Soc.* **145,** 2088–2092; 10.1021/jacs.2c13232 (2023).
44. Berg, W. R. *et al.* Light-Activated Assembly of DNA Origami into Dissipative Fibrils. *Angew. Chem. Int. Ed.* **62,** e202314458; 10.1002/anie.202314458 (2023).
45. Selmani, S. *et al.* Electrically Fueled Active Supramolecular Materials. *J. Am. Chem. Soc.* **144,** 7844–7851; 10.1021/jacs.2c01884 (2022).

46. Barpuzary, D., Hurst, P. J., Patterson, J. P. & Guan, Z. Waste-Free Fully Electrically Fueled Dissipative Self-Assembly System. *J. Am. Chem. Soc.* **145,** 3727–3735; 10.1021/jacs.2c13140 (2023).
47. Baretta, R. & Frasconi, M. Electrically Powered Dissipative Hydrogel Networks Reveal Transient Stiffness Properties for Out-of-Equilibrium Operations. *J. Am. Chem. Soc.* **146,** 7408–7418; 10.1021/jacs.3c12653 (2024).
48. Chen, C. & Guan, Z. Precise Control of Dissipative Self-assembly by Light and Electricity. *Chem. Eur. J.* **29,** e202300347; 10.1002/chem.202300347 (2023).
49. Valentini, M. *et al.* A Doubly Dissipative System Driven by Chemical and Radiative Stimuli. *Chem. Eur. J.* **29,** e202301835; 10.1002/chem.202301835 (2023).
50. Alvarez-Lorenzo, C., Bromberg, L. & Concheiro, A. Light-sensitive intelligent drug delivery systems. *Photochem. Photobiol.* **85,** 848–860; 10.1111/j.1751-1097.2008.00530.x (2009).
51. Groeneveld, I., Kanelli, M., Ariese, F. & van Bommel, M. R. Parameters that affect the photodegradation of dyes and pigments in solution and on substrate – An overview. *Dyes Pigment.* **210,** 110999; 10.1016/j.dyepig.2022.110999 (2023).
52. Yun, S. H. & Kwok, S. J. J. Light in diagnosis, therapy and surgery. *Nat. Biomed. Eng.* **1,** 8; 10.1038/s41551-016-0008 (2017).
53. Yi, Y. *et al.* Electrochemical corrosion of a glassy carbon electrode. *Catal. Today* **295,** 32–40; 10.1016/j.cattod.2017.07.013 (2017).
54. Singh, S., Srivastava, V. C. & Mall, I. D. Mechanism of Dye Degradation during Electrochemical Treatment. *J. Phys. Chem. C* **117,** 15229–15240; 10.1021/jp405289f (2013).
55. Suslick, K. S. Sonochemistry. *Science* **247,** 1439–1445; 10.1126/science.247.4949.1439 (1990).
56. Jiang, S., Late, E. K. Y., Jeromé, F., Amaniampong, P. N. & Mushrif, S. H. Ultrasound-Assisted Catalysis: A Pathway to Novel and Selective Chemical Transformations in Condensed Phase. *ChemistrySelect* **9,** e202401953; 10.1002/slct.202401953 (2024).
57. Sun, J. *et al.* Ultrasound-induced single-electron reduction of azide groups in aromatic prodrugs. *Natl. Sci. Rev.* **12,** nwaf140; 10.1093/nsr/nwaf140 (2025).
58. Hickenboth, C. R. *et al.* Biasing reaction pathways with mechanical force. *Nature* **446,** 423–427; 10.1038/nature05681 (2007).
59. Li, J., Nagamani, C. & Moore, J. S. Polymer mechanochemistry: from destructive to productive. *Acc. Chem. Res.* **48,** 2181–2190; 10.1021/acs.accounts.5b00184 (2015).
60. Akbulatov, S. & Boulatov, R. Experimental Polymer Mechanochemistry and its Interpretational Frameworks. *ChemPhysChem* **18,** 1422–1450; 10.1002/cphc.201601354 (2017).
61. Klok, H.-A., Herrmann, A. & Göstl, R. Force ahead: Emerging Applications and Opportunities of Polymer Mechanochemistry. *ACS Polym. Au* **2,** 208–212; 10.1021/acspolymersau.2c00029 (2022).
62. Bo, G. de. Polymer Mechanochemistry and the Emergence of the Mechanophore Concept. *Macromolecules* **53,** 7615–7617; 10.1021/acs.macromol.0c01683 (2020).

63. Piermattei, A., Karthikeyan, S. & Sijbesma, R. P. Activating catalysts with mechanical force. *Nat. Chem.* **1,** 133–137; 10.1038/nchem.167 (2009).
64. Michael, P. & Binder, W. H. A Mechanochemically Triggered "Click" Catalyst. *Angew. Chem. Int. Ed.* **54,** 13918–13922; 10.1002/anie.201505678 (2015).
65. Campagna, D. & Göstl, R. Mechanoresponsive Carbamoyloximes for the Activation of Secondary Amines in Polymers. *Angew. Chem. Int. Ed.* **61,** e202207557; 10.1002/anie.202207557 (2022).
66. Ramirez, A. L. B. *et al.* Mechanochemical strengthening of a synthetic polymer in response to typically destructive shear forces. *Nat. Chem.* **5,** 757–761; 10.1038/nchem.1720 (2013).
67. Zhang, H. *et al.* Mechanochromism and Mechanical-Force-Triggered Cross-Linking from a Single Reactive Moiety Incorporated into Polymer Chains. *Angew. Chem. Int. Ed.* **55,** 3040–3044; 10.1002/anie.201510171 (2016).
68. Hu, X., Zeng, T., Husic, C. C. & Robb, M. J. Mechanically Triggered Small Molecule Release from a Masked Furfuryl Carbonate. *J. Am. Chem. Soc.* **141,** 15018–15023; 10.1021/jacs.9b08663 (2019).
69. Shi, Z., Wu, J., Song, Q., Göstl, R. & Herrmann, A. Toward Drug Release Using Polymer Mechanochemical Disulfide Scission. *J. Am. Chem. Soc.* **142,** 14725–14732; 10.1021/jacs.0c07077 (2020).
70. Shi, Z., Song, Q., Göstl, R. & Herrmann, A. Mechanochemical activation of disulfide-based multifunctional polymers for theranostic drug release. *Chem. Sci.* **12,** 1668–1674; 10.1039/D0SC06054B (2020).
71. Zeng, T., Ordner, L. A., Liu, P. & Robb, M. J. Multimechanophore Polymers for Mechanically Triggered Small Molecule Release with Ultrahigh Payload Capacity. *J. Am. Chem. Soc.* **146,** 95–100; 10.1021/jacs.3c11927 (2024).
72. Chen, L., Nixon, R. & Bo, G. de. Force-controlled release of small molecules with a rotaxane actuator. *Nature* **628,** 320–325; 10.1038/s41586-024-07154-0 (2024).
73. He, S., Stratigaki, M., Centeno, S. P., Dreuw, A. & Göstl, R. Tailoring the Properties of Optical Force Probes for Polymer Mechanochemistry. *Chem. Eur. J.* **27,** 15889–15897; 10.1002/chem.202102938 (2021).
74. Asya, B. V., Wang, S., Euchler, E., Khiêm, V. N. & Göstl, R. Optical Force Probes for Spatially Resolved Imaging of Polymer Damage and Failure. *Aggregate* **6,** e70014; 10.1002/agt2.70014 (2025).
75. Huo, S. *et al.* Mechanochemical bond scission for the activation of drugs. *Nat. Chem.* **13,** 131–139; 10.1038/s41557-020-00624-8 (2021).
76. Yildiz, D., Göstl, R. & Herrmann, A. Sonopharmacology: controlling pharmacotherapy and diagnosis by ultrasound-induced polymer mechanochemistry. *Chem. Sci.* **13,** 13708–13719; 10.1039/D2SC05196F (2022).
77. Xuan, M. *et al.* Polymer Mechanochemistry in Microbubbles. *Adv. Mater.* **35,** e2305130; 10.1002/adma.202305130 (2023).

78. Fan, J. *et al.* Polymer microbubbles as universal platform to accelerate polymer mechanochemistry. *Nat. Commun.* **16,** 5380; 10.1038/s41467-025-60667-8 (2025).
79. Ishaqat, A. *et al.* In Vivo Polymer Mechanochemistry with Polynucleotides. *Adv. Mater.* **36,** e2403752; 10.1002/adma.202403752 (2024).
80. May, P. A. & Moore, J. S. Polymer mechanochemistry: techniques to generate molecular force via elongational flows. *Chem. Soc. Rev.* **42,** 7497–7506; 10.1039/C2CS35463B (2013).
81. Boulatov, R. *Polymer Mechanochemistry* (Springer International Publishing, Cham, 2015).
82. Ren, Y. & You, L. Dynamic signaling cascades: reversible covalent reaction-coupled molecular switches. *J. Am. Chem. Soc.* **137,** 14220–14228; 10.1021/jacs.5b09912 (2015).
83. Montoya, L. A. & Pluth, M. D. Selective turn-on fluorescent probes for imaging hydrogen sulfide in living cells. *Chem. Comm.* **48,** 4767–4769; 10.1039/c2cc30730h (2012).
84. Weil, T., Vosch, T., Hofkens, J., Peneva, K. & Müllen, K. The rylene colorant family--tailored nanoemitters for photonics research and applications. *Angew. Chem. Int. Ed.* **49,** 9068–9093; 10.1002/anie.200902532 (2010).
85. Roy, R., Khan, A., Chatterjee, O., Bhunia, S. & Koner, A. L. Perylene Monoimide as a Versatile Fluoroprobe: The Past, Present, and Future. *Org. Mater.* **3,** 417–454; 10.1055/a-1551-6930 (2021).
86. Gong, W.-L., Xiong, Z.-J., Li, C. & Zhu, M.-Q. Design, synthesis and photoswitching of broad-spectrum fluorescent hexaarylbiimidazoles. *RSC Adv.* **4,** 64371–64378; 10.1039/C4RA10451J (2014).
87. Hayes, R. T., Wasielewski, M. R. & Gosztola, D. Ultrafast Photoswitched Charge Transmission through the Bridge Molecule in a Donor–Bridge–Acceptor System. *J. Am. Chem. Soc.* **122,** 5563–5567; 10.1021/ja000219d (2000).
88. Becker, S., Böhm, A. & Müllen, K. New Thermotropic Dyes Based on Amino-Substituted Perylendicarboximides. *Chem. Eur. J.* **6,** 3984–3990; 10.1002/1521-3765(20001103)6:21<3984::AID-CHEM3984>3.0.CO;2-F (2000).
89. Bissell, R. A., Córdova, E., Kaifer, A. E. & Stoddart, J. F. A chemically and electrochemically switchable molecular shuttle. *Nature* **369,** 133–137; 10.1038/369133a0 (1994).
90. Kwan, C.-S., Chan, A. S. C. & Leung, K. C.-F. A Fluorescent and Switchable Rotaxane Dual Organocatalyst. *Org. Lett.* **18,** 976–979; 10.1021/acs.orglett.5b03700 (2016).
91. Biagini, C. *et al.* Dissipative Catalysis with a Molecular Machine. *Angew. Chem. Int. Ed.* **58,** 9876–9880; 10.1002/anie.201905250 (2019).
92. Zheng, T., Wang, X., Ng, W.-H., Tse, Y.-L. S. & Yeung, Y.-Y. Catalytic enantio- and diastereoselective domino halocyclization and spiroketalization. *Nat. Catal.* **3,** 993–1001; 10.1038/s41929-020-00530-9 (2020).
93. Rueping, M. *et al.* Nature-inspired cascade catalysis: reaction control through substrate concentration--double vs. quadruple domino reactions. *Chem. Comm.* **47,** 3828–3830; 10.1039/C1CC10245A (2011).

94. Mattia, E. & Otto, S. Supramolecular systems chemistry. *Nat. Nanotechnol.* **10,** 111–119; 10.1038/nnano.2014.337 (2015).
95. Ruangsupapichat, N., Pollard, M. M., Harutyunyan, S. R. & Feringa, B. L. Reversing the direction in a light-driven rotary molecular motor. *Nat. Chem.* **3,** 53–60; 10.1038/nchem.872 (2011).
96. McNamara, L. E. *et al.* Bright, Modular, and Switchable Near-Infrared II Emission from Compact Tetrathiafulvalene-Based Diradicaloid Complexes. *J. Am. Chem. Soc.* **144,** 16447–16455; 10.1021/jacs.2c04976 (2022).
97. Mao, J. *et al.* Near-Infrared Blinking Carbon Dots Designed for Quantitative Nanoscopy. *Nano Lett.* **23,** 124–131; 10.1021/acs.nanolett.2c03711 (2023).
98. Mengji, R., Acharya, C., Vangala, V. & Jana, A. A lysosome-specific near-infrared fluorescent probe for in vitro cancer cell detection and non-invasive in vivo imaging. *Chem. Comm.* **55,** 14182–14185; 10.1039/C9CC07322A (2019).
99. Norel, L., Galangau, O., Al Sabea, H. & Rigaut, S. Remote Control of Near Infrared Emission with Lanthanide Complexes. *ChemPhotoChem* **5,** 393–405; 10.1002/cptc.202000248 (2021).
100. Fulmer, G. R. *et al.* NMR Chemical Shifts of Trace Impurities: Common Laboratory Solvents, Organics, and Gases in Deuterated Solvents Relevant to the Organometallic Chemist. *Organometallics* **29,** 2176–2179; 10.1021/om100106e (2010).

Figures

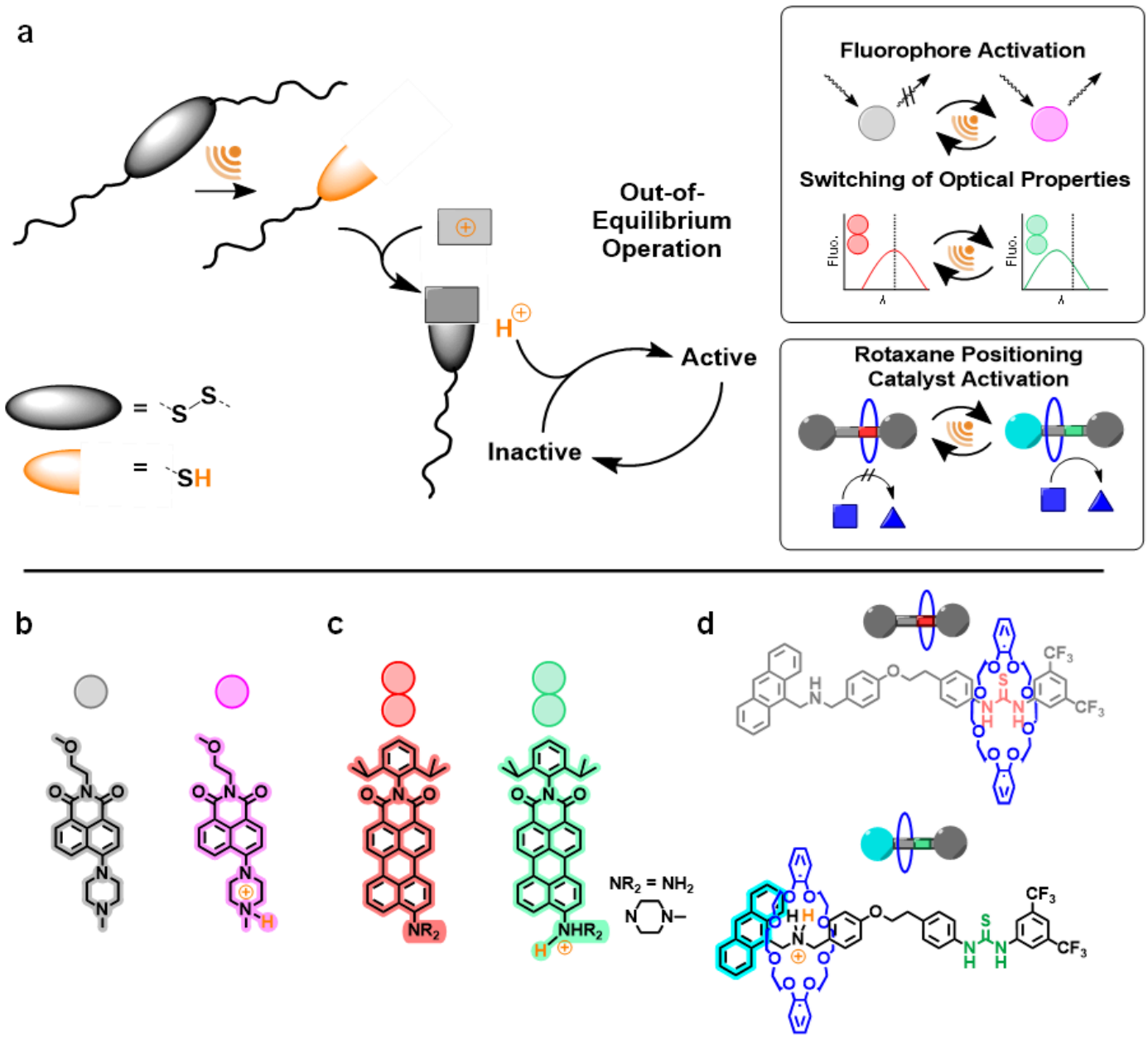


Figure 1

Ultrasound-driven dissipative reaction networks for controlling optical functionalities and catalysis. a, Ultrasound-induced cleavage of disulfide mechanophores generates thiols that induce proton release from a molecular switch, thereby activating distinct latent functionalities according to the respective network design. These functionalities revert to their initial states in the presence of an organic base, and the cycles can be re-initiated by further ultrasound exposure, enabling externally regulatable out-of-equilibrium chemistry. b,Molecular structures of the naphthalimide-based fluorophore in its inactive (deprotonated) and active (protonated) states. c, Molecular structures of the perylene monoimide (PMI)-based NIR emitter in its red-shifted (deprotonated) and green-shifted (protonated) states. A primary or tertiary amine is attached to the PMI. d, Molecular structures of the [2]rotaxane in its catalytically inactive, non-fluorescent (deprotonated) state and catalytically active, fluorescent (protonated) state.

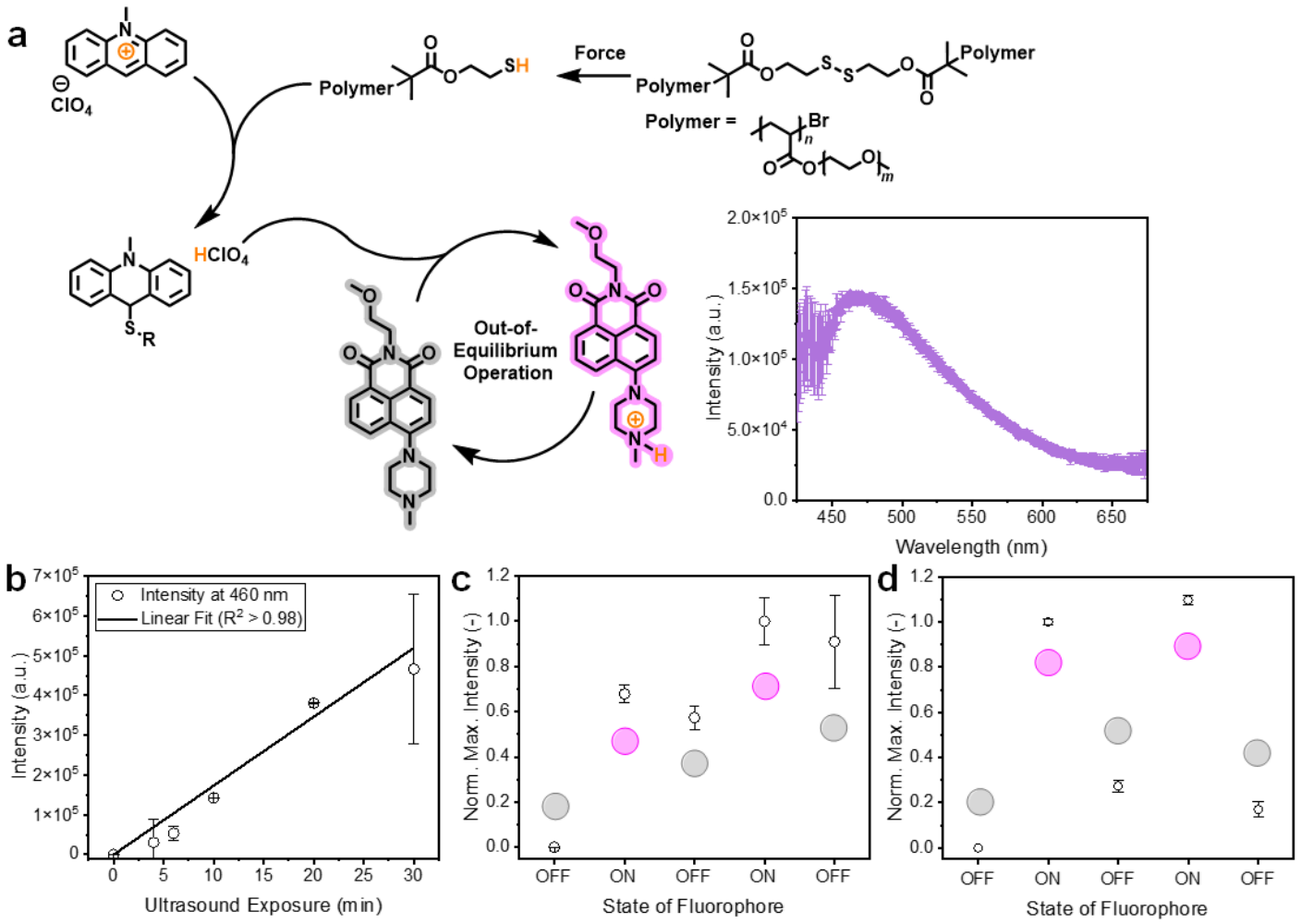


Figure 2

Ultrasound-driven dissipative activation of fluorescence. a, Reaction scheme of activation and dissipation-induced deactivation of the fluorescent state of a naphthalimide fluorophore. The corresponding fluorescence spectrum shows the switched-on state of the fluorophore with an emission maximum at ~ 460 nm. b, Linear correlation plot at 460 nm establishing ultrasound-exposure-dependent fluorescence. c, Normalized fluorescence plot demonstrating switchability between the OFF state (grey) and the ON state (purple) of the fluorophore. The OFF state was attained by keeping the solution in the dark at room temperature for 5 days. d, Normalized fluorescence plot establishing switching between the OFF state (grey) and the ON state (purple) of the fluorophore. Here, the OFF state was realized by introducing 0.5 equivalents of TBD into the reaction mixture. The concentration of fluorophore and molecular switch was 4.0 μM, and the concentration of the disulfide-containing polymer was 6.0 μM for all the experiments (a-d). Error bars represent standard deviations derived from independent sonication experiments. The fluorescence data (a-d) were obtained after subjecting the reaction mixture to ultrasound for 10 minutes, recorded at an excitation wavelength of 360 nm, with a spectral bandwidth of 3 nm, unless noted otherwise.

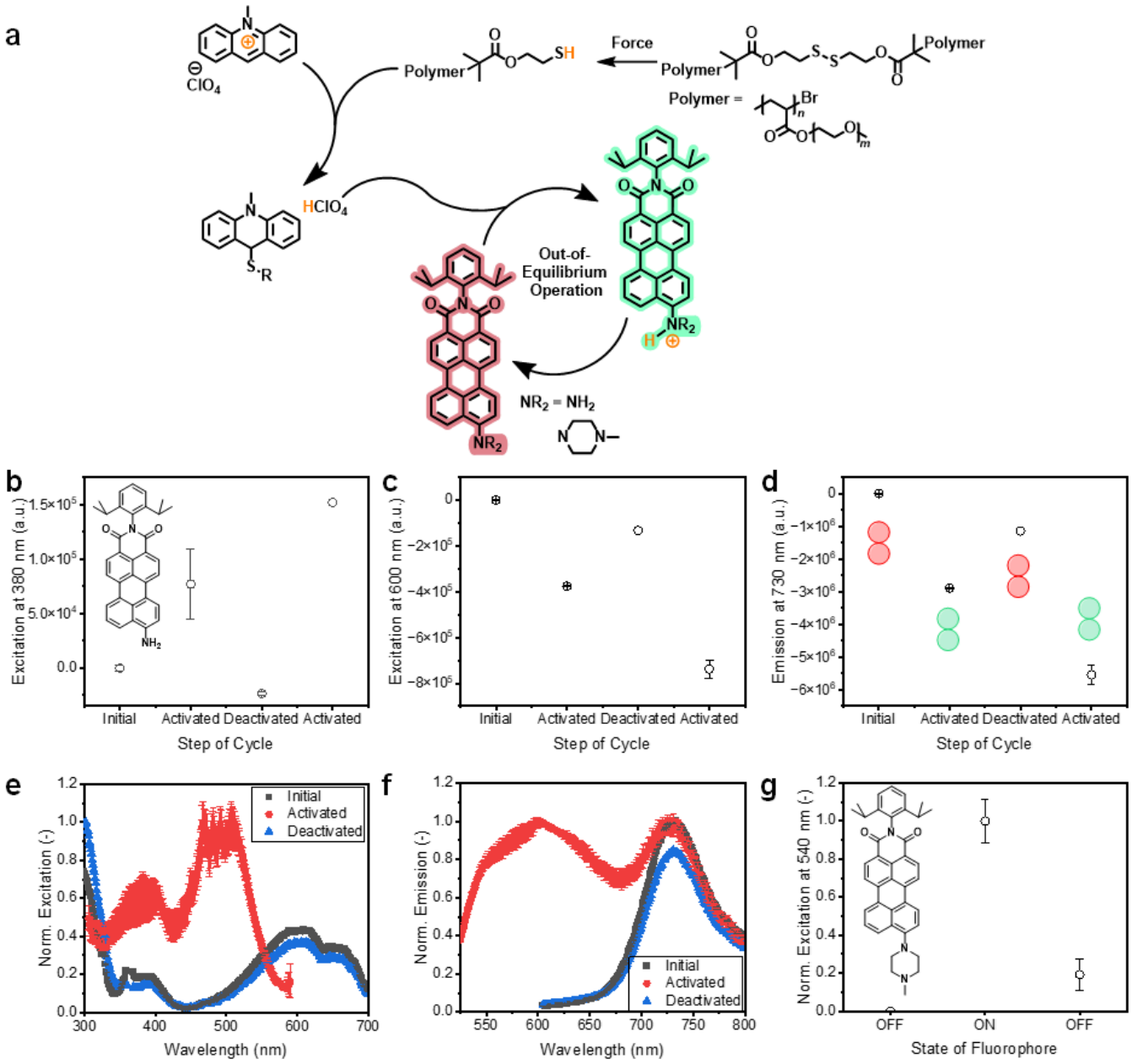


Figure 3

Ultrasound-triggered dissipative modulation of the optical behavior of perylene-based NIR emitters. a, Reaction scheme depicting the out-of-equilibrium switching of the fluorescence of primary (1°) and tertiary (3°) PMI amine fluorophores. b, Mechanochemically fueled activation of the low-wavelength excitation state of 1° PMI amine recorded at 600 nm emission wavelength. c, Mechanochemical control over the deactivation of high-wavelength excitation of 1° PMI amine monitored at 730 nm emission wavelength. d, Mechanodissipative switching between the NIR active (red) and inactive (green) states of 1° PMI amine measured at an excitation wavelength of 590 nm. e, Representative normalized excitation spectra of the initial reaction mixture, the activated (after ultrasound exposure), and deactivated (0.5 equivalent TBD) states of 1° PMI amine recorded at 730 nm emission wavelength. f, Representative normalized fluorescence spectra of the initial reaction mixture, the activated (after ultrasound exposure),

and deactivated (0.5 equivalent TBD) states of 1° PMI amine monitored at 510 nm emission wavelength. g, Normalized excitation plot showcasing switching between the OFF state and the ON state of the 3° PMI amine fluorophore at 730 nm emission wavelength. In all the experiments, the concentrations of the fluorophore, molecular switch, disulfide-centered polymer, and TBD were 2.0 μM, 4.0 μM, 6.0 μM, and 1.0 μM, respectively. The TBD was added after the initial fueling step in the cascade. Error bars represent standard deviations derived from independent sonication experiments. The optical data (b-c and e-g) were obtained with a spectral bandwidth of 3 nm. The switching between the NIR active and inactive states of 1° PMI amine shown in Fig. d was obtained with a spectral bandwidth of 5 nm. All spectra were recorded after subjecting the respective reaction mixture to ultrasound for 10 minutes.

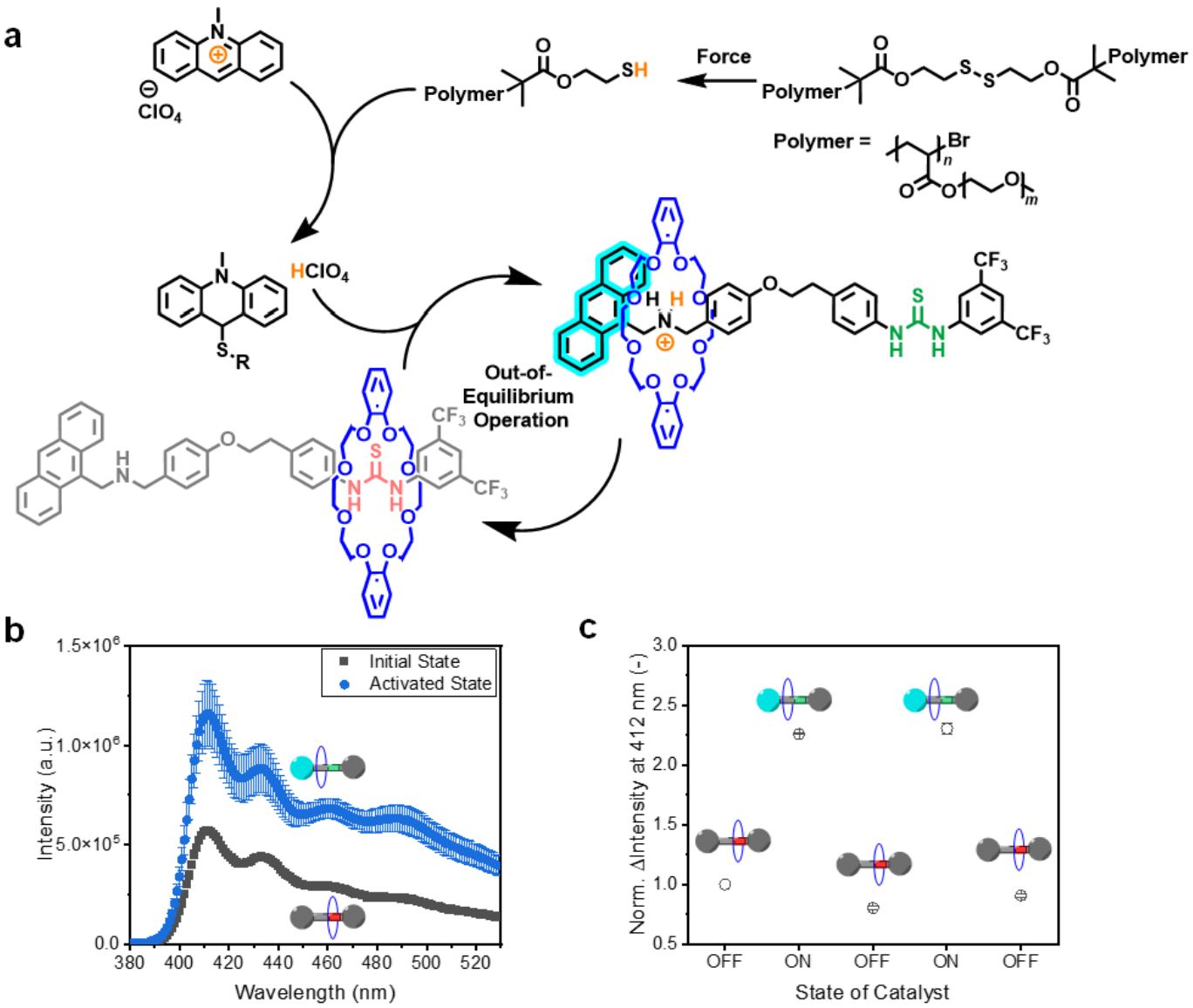


Figure 4

Force-governed transient positioning of a macrocyclic rotaxane. a, Reaction scheme of fueling the dissipative uncaging of a thiourea unit by controlling the positioning of a macrocycle in a [2]rotaxane. b,

Representative fluorescence spectra of the initial (thiourea caged) and the activated (thiourea uncaged) states informing the macrocycle position relative to the anthracene cap. A higher fluorescence confirms a closer position of the macrocycle to the anthracene. c, Normalized difference in fluorescence intensity obtained at 412 nm showing the switchable positioning of the macrocycle. For all the experiments, the concentrations of [2]rotaxane, molecular switch, disulfide mechanophore-containing polymer, and TBD were 1.0 μM, 6.0 μM, 180 μM, and 3.0 μM, respectively. The TBD was added after the initial fueling step in the cascade. Error bars represent standard deviations derived from independent sonication experiments. The fluorescence data were obtained after subjecting the reaction mixture to ultrasound for 10 minutes, recorded at an excitation wavelength of 368 nm, with a spectral bandwidth of 2 nm.

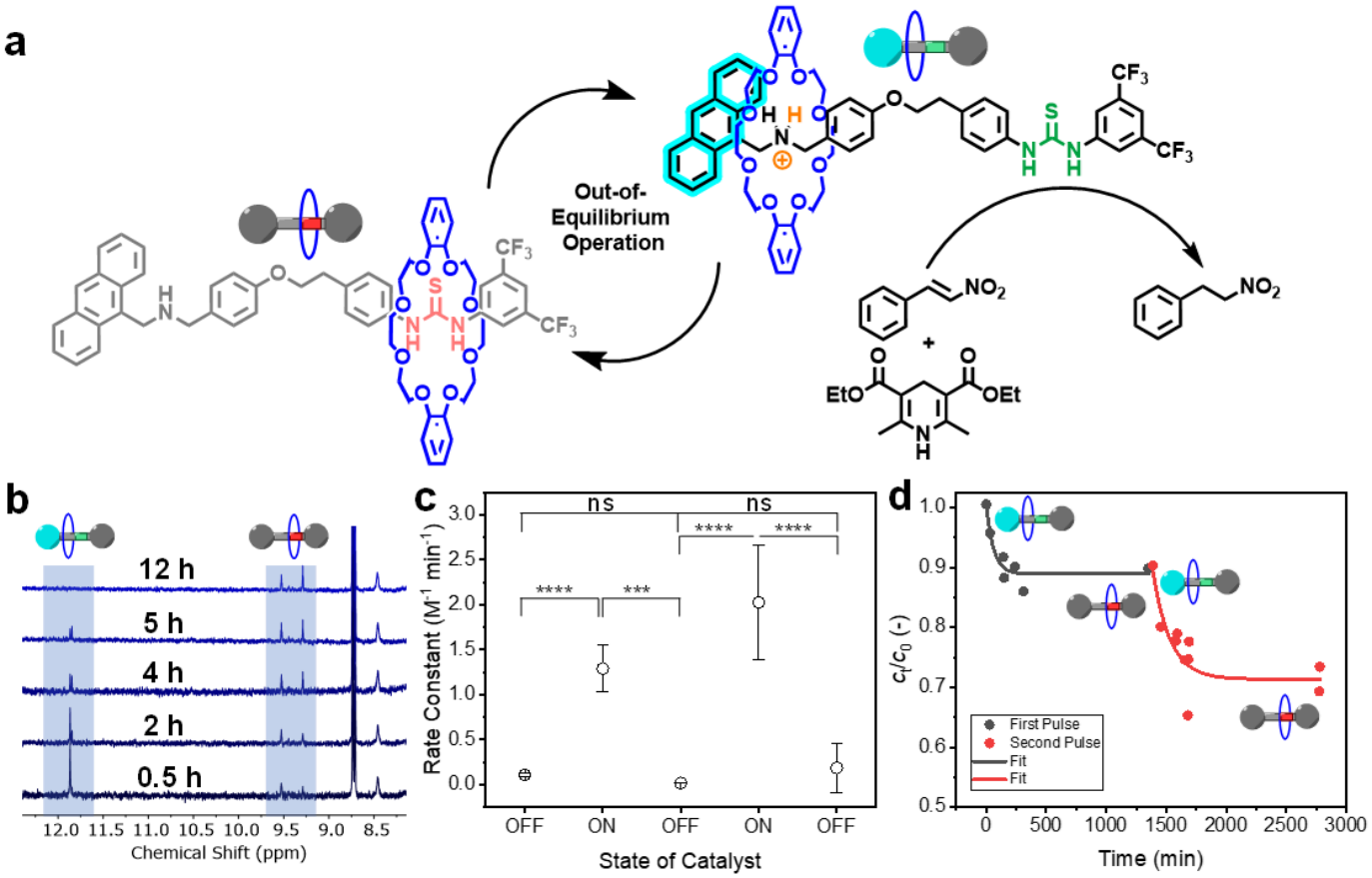


Figure 5

Ultrasound-triggered dissipative catalysis with a rotaxane. a, Reaction scheme illustrating the dissipative switching of the macrocycle position in a [2]rotaxane to transiently uncage a thiourea motif, which catalyzes the biomimetic hydrogenation of nitrostyrene. The fueling reaction shown in Fig. 4 has been omitted here for clarity. b, Stacked ^{1}H NMR spectra displaying the signals of the activated state (uncaged thiourea, s to d, 11.8 ppm) and the deactivated state (caged thiourea, d, 9.5 and 9.25 ppm) at different reaction times (0.5-12 h). c, Second-order rate constants for the biomimetic hydrogenation reaction of the [2]rotaxane in the initial state, the activated state (after 10 minutes of ultrasound), and the deactivated state (after 12 h). **** indicates $p < 0.001$, and *** indicates $p < 0.005$. Error bars represent

standard deviations from three independent sonication experiments. d, Conversion (c_t/c_0) of the nitrostyrene starting material over time after the first (black) and second (red) ultrasound exposures (10 minutes each). Data points represent merged results from three independent experiments. An exponential function was fitted to account for the decrease in reaction rate due to catalyst deactivation over time.

Supplementary Files

This is a list of supplementary files associated with this preprint. Click to download.

- NatChemUltrasounddriveschemicalsystemsoutofequilibriumSI.pdf